Research Article

Biosynthesis of Cu_4O_3 nanoparticles using *Razma* seeds: application to antibacterial and cytotoxicity activities

J. Thanuja[1] · Udayabhanu[2] · G. Nagaraju[2] · H. Raja Naika[1]

Received: 14 March 2019 / Accepted: 22 October 2019 / Published online: 20 November 2019

Abstract
In the present work, Cu_4O_3 nanoparticles were prepared by biosynthesis method using *Razma* seeds and copper sulfate as a precursors. The synthesized Cu_4O_3 nanoparticles were characterized using various analytical tools such as XRD, FTIR, UV–Vis, SEM and TEM. The average crystallite size of the prepared Cu_4O_3 nanoparticles was calculated by Debye–Scherrer's equation and found to be 13 nm. The TEM images clearly reveal the average size of the particles is 27 nm. Antibacterial activity of Cu_4O_3 nanoparticles was tested against Gram-positive (*Staphylococcus aureus*) and Gram-negative (*Escherichia coli*) bacteria by agar well diffusion method. The cytotoxic activity of synthesized Cu_4O_3 nanoparticles was examined against human prostate cancer cells (PC-3). The prepared NPs show the significant antioxidant activity through scavenging of 1,1-diphenyl-2-picrylhydrazyl free radicals.

Keywords Biosynthesis · Cu_4O_3 · Antibacterial · Anticancer · Antioxidant

1 Introduction

Cancer is one of the leading diseases which will cause global death rates up to 15 million by 2020 and is characterized by proliferation of abnormal cells. Every year, more than 11 million people are diagnosed with cancer across the world [1, 2]. Cancer (uncontrolled cell growth) is one of the major diseases that affect humans and more than 20% of the world's population. There are 200 different types of cancers found across the world which was surveyed by the World Health Organization (WHO) [3]. Uncontrolled growth of cells leads to mutation in genes, which causes cancer by accelerating cell division rates or inhibiting normal controls or programmed cell death. Prostate cancer was the second most commonly diagnosed cancer in men. Thus, many studies have focused on the developing anticancer agents to treat prostate cancer. Prostate cancer affects the prostate gland that produces some of the fluid in semen and plays a role in urine control. In this aspect, identification of novel compounds to include antimicrobial, antioxidant and anticancer activities would be of greater commercial value to the today's pharmaceutical industry [4].

In addition, the consumption of contaminated food causes serious illnesses throughout the world, where the contamination of food with pathogenic bacteria such as *Staphylococcus aureus* and *Escherichia coli* is a serious public health problem [5–7]. Food-borne pathogens have recently become the most common global public health problem [8, 9]. Therefore, in order to overcome this problem, it is necessary to develop novel inorganic antibacterial agents to combat *S. aureus* and *E. coli*. Metal oxide nanoparticles, CeO_2, MgO and Fe_3O_4 have good antibacterial activities, but they are not highly effective against food-borne pathogens. $Ca(OH)_2$ NPs shows better antibacterial efficiency [10]. ZnO nanoparticles showed antimicrobial potential against the food-borne pathogens [11]. The study of antioxidant property of nanoparticles has

✉ H. Raja Naika, rajanaik1100@gmail.com | [1]Department of Studies and Research in Biotechnology, Tumkur University, Tumakuru 572 103, India. [2]Energy Materials Research Laboratory, Department of Chemistry, Siddaganga Institute of Technology, Tumakuru 572 103, India.

become one of the significant basic studies in pharmaceutical science and nanoscience. Polyphenolic and flavonoid compounds acts as strong antioxidants, and they are responsible for various biological activities like anticancer, anti-inflammatory and antifungal properties [12]. An antioxidant is a compound that delays or prevents the oxidation of an oxidizable species. Oxidative stress, induced by reactive oxygen species (ROS) produced in the body, is one of the main factors of current slow killer diseases that population is suffering from such as cancer, diabetes, cardiovascular neurological (Alzheimer's and Parkinson's) inflammatory viral diseases and digestive disorders [13].

Copper oxide nanostructures have attracted significant attention because of their wide range of applications. The metal oxide nanoparticles are of particular interest as they exhibit unique phenomenal properties [14]. Copper is an abundantly available multivalent metal that reacts readily with oxygen to form three phases of oxide: CuO (tenorite), Cu_2O (cuprite) and Cu_4O_3 (paramelaconite) [15]. Among three phases, Cu_4O_3 phase (paramelaconite is a natural and very scarce mineral) is very rare and difficult to synthesize. Cu_4O_3 contains both Cu(I) and Cu(II) oxidation states [16]. The synthesis of bulk Cu_4O_3 through the conventional chemical routes is rather challenging, because it is very difficult to stabilize the Cu^{2+} and Cu^{+} ions simultaneously. Paramelaconite Cu_4O_3 is a metastable copper oxide with a copper-to-oxygen atomic ratio of 1.33, leading to the formula Cu_4O_3 [17].

The applications include: spintronic devices, anode materials for lithium-ion batteries, photocatalysis, solar cells, tribology and high-temperature superconductivity. The recent research articles on Cu_4O_3 clearly bring out the present state of understanding on their synthesis, optical and electrical properties and their applications [18]. Cu_4O_3 is a p-type semiconductor with a direct band gap of 2.34 eV and an indirect band gap of 1.50 eV [19]. The binary family of cuprous oxide (Cu_2O), cupric oxide (CuO) and paramelaconite (Cu_4O_3) has numerous functional applications due to their unique structures and electronic configurations [20]. Paramelaconite Cu_4O_3 is a mineral that shows puzzling magnetic properties. The crystal structure and the magnetic properties of Cu_4O_3 have been studied using single-crystal mineral samples [21]. Cu_4O_3 material could provide opportunities to further explore its physicochemical properties and potential biological applications [22]. Copper oxide NPs posses significant antimicrobial properties by inhibiting the growth of bacteria, viruses, fungi and algae [23, 24]. In the present work, the green synthesis of copper oxide nanoparticles using aqueous extract of *Cicer arietinum* (Razma seed) is an alternative to chemical methods studied. Their antibacterial (foodborne), antiproliferative and antioxidant activities against prostate cancer cell line were investigated.

2 Materials and methods

$CuSO_4$ was purchased from SD Fine Chemicals Ltd., Mumbai; *Razma* seeds were collected from a local supermarket in Tumkur.

2.1 Preparation of the extract

20 grams collected Razma seeds was powdered using mixer grinder. The powder was added to 500-mL round-bottomed flask containing 400 mL of distilled water. The solution mixture was heated for 30 min at 85 °C to get complete extraction. Afterward, the extraction mixture was filtered, dried and used for the synthesis of Cu_4O_3 NPs.

2.2 Synthesis of Cu_4O_3 nanoparticles

To synthesize Cu_4O_3 nanoparticles (NPs), 100 mg of Razma seed extract was added to 90 mL of 5 mM $CuSO_4$ at ambient temperature, stirred continuously for 20 min in magnetic stirrer to mix the metal precursor completely and kept for reflux with vigorous stirring at 97 °C for 8 h. The reaction mixture was cooled to room temperature, then dried in hot air oven at 90 °C for 24 h and stored in airtight vials.

2.3 Characterization

Phase purity and crystallite size were determined by X-ray diffraction (Rigaku Smart Lab X-ray diffractometer) (Cu-kα $\lambda = 1.540$ Å). The stretching frequencies of functional groups were confirmed by Bruker Alpha FTIR spectrometer by KBr pellet method in the range of 4000–400 cm^{-1}. The morphology of the NPs was assessed by scanning electron microscopy (Gemini-Ultra 55) and the chemical composition by energy-dispersive X-ray analysis (EDAX). Particle sizes were characterized by JEOL 2100 high-resolution transmission electron microscopy (HR-TEM). The optical properties of Cu_4O_3 NPs were measured using UV–visible spectrophotometer (Agilent carry-60).

2.4 Antibacterial assay

Antibacterial activity was screened against Gram-positive *Staphylococcus aureus* (*S. aureus*) *and* Gram-negative *Escherichia coli* (*E. coli*) bacteria (NCIM-5022) by agar well diffusion method. Nutrient agar plates were prepared and swabbed using sterile L-shaped glass rod. 100 µL of 24-h mature broth culture of individual bacterial strains was smeared on the plates. The wells were made by using sterile cork borer (6 mm) into petri

Table 1 Antibacterial activity of Cu_4O_3 nanoparticles against pathogenic bacteria

Pathogens	Zone of inhibition (mm)			
	200 µg/mL	400 µg/mL	600 µg/mL	Standard (ciprofloxacin) (5 µg/mL)
E. coli	0	10 ± 0.2	6	20
S. aureus	0	5	10	20

plates, and varied concentrations of Cu_4O_3 NPs (200, 400, 600 µg/well) were used to assess the activity of the NPs. The compounds were dispersed in sterile water and they were used as a negative control and ciprofloxacin (5 µg/50 µL) was used as positive control and these petri plates were incubated at 37 °C for 36 h. From these petri plates, the developed zone of inhibition of every well was measured in millimeter (mm) and the values are given in Table 1 [25, 26].

2.5 Anticancer activity assay

The cells were trypsinized and aspirated into a 15-mL centrifuge tube. Cell pellet was obtained by centrifugation at 300 rpm. The cell count was adjusted, using DMEM HG medium, such that 200 µL of suspension contained approximately 10,000 cells. To each well of the 96-well microtitre plate, 200 µL of the cell suspension was added and the plate was incubated at 37 °C and the 5% CO_2 atmosphere was maintained for 24 h. After incubation, the spent medium was aspirated. 200 µL of different test concentrations (20, 40, 60, 80 and 100 µg/mL) from stock test drugs was added to the respective wells. The plate was again incubated at 37 °C with 5% CO_2 atmosphere for 24 h. Then the plate was removed from the incubator, and the drug-containing media was aspirated. 200 µL of medium containing 10% MTT reagent was then added to each well to get a final concentration of 0.5 mg/mL, and the plate was incubated at 37 °C and 5% CO_2 atmosphere for 3 h. The culture medium was removed completely without disturbing the crystals formed. Then 100 µL of solubilization solution (DMSO) was added, and the plate was gently shaken in a gyratory shaker to solubilize the formed formazan. The absorbance was measured using a microplate reader at a wavelength of 570 nm and also at 630 nm. The percentage growth inhibition was calculated, after subtracting the background and the blank. The inhibition concentration 50% (IC_{50}) value was calculated from the dose–response curve of the cell lines [27].

2.6 Antioxidant activity assay

Antioxidant activity was carried out by 1,1-diphenyl-2-picrylhydrazyl (DPPH) assay using the Brand Williams method [28]. DPPH (oxidized form) is a stable free radical with purple color having absorption maximum at 520 nm, in the presence of an antioxidant which can donate an electron to DPPH radical for inhibiting the activity of DPPH molecule. This results in the change in absorbance at 520 nm. DPPH (39.4 mg) was dissolved in 100 mL of methanol to get 0.14 mM concentration in the assay. Ascorbic acid was used as standard, and without adding nanoparticles, the solution was treated as a positive control. 1 mM DPPH was mixed with varied concentration of nanoparticle solution—136, 221, 306, 391, 476 and 561 µg/mL—and incubated at 37 °C for 30 min. The absorbance was recorded at 520 nm against 50% methanol blank using the UV–visible spectrophotometer. The antioxidant activity was measured by taking the absorbance difference of the control and the nanoparticle solution. The % inhibition was calculated by Eq. (1). The IC_{50} value was determined by plotting the line at 50% inhibition (*y*-axis) to the concentration of nanoparticle solution (*x*-axis) [29, 30].

$$\% \text{ Inhibition} = \frac{\text{Absorbance (control)} - \text{Absorbance (Test)}}{\text{Absorbance (control)}} \times 100 \quad (1)$$

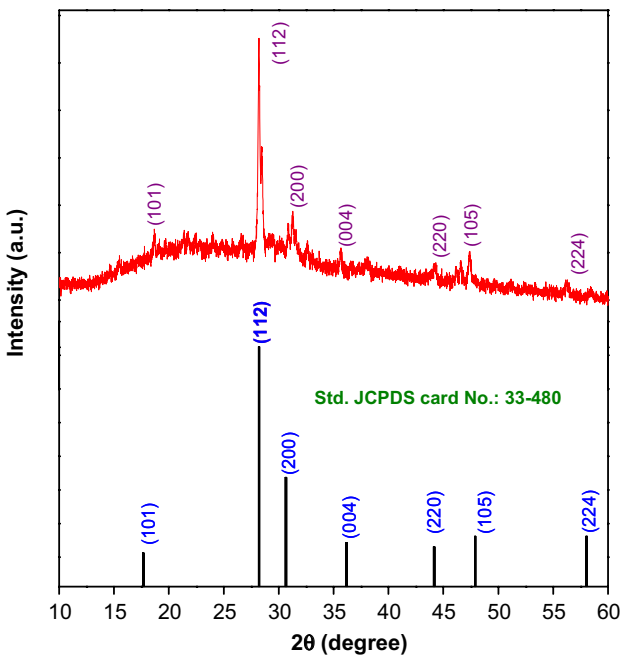

Fig. 1 XRD pattern of synthesized Cu_4O_3 nanoparticles

3 Results and discussion

3.1 XRD structural analysis

Figure 1 shows the XRD patterns of Cu_4O_3 NPs. The XRD peak positions were consistent with the standard Cu_4O_3, and sharp peaks in the diffraction pattern indicate the crystalline structure. These are in good agreement with the standard JCPDS card No. 33-480. It belongs to tetragonal copper oxide paramelaconite. No impurity peaks other than Cu_4O_3 were observed in XRD, indicating the purity of the sample. The average crystallite size of the Cu_4O_3 NPs was calculated by Debye–Scherrer's equation (2).

$$D = k\lambda / \beta \cos\theta \tag{2}$$

where D is the particle size (nm), λ is the wavelength of the X-ray, K is a constant (0.94), β is the full width at half maximum of the peak (in radians) and 2θ is the Bragg angle (°). The average crystallite size (D) of tetragon-shaped Cu_4O_3 was found to be 13 nm.

3.2 FTIR analysis

Figure 2 shows the FTIR spectrum of Cu_4O_3 NPs synthesized using Razma seed extract. These NPs have shown absorption band at 3416 cm^{-1} which corresponds to –OH stretching, and band at 1638 cm^{-1} was related to –OH bending frequency of surface hydroxyl groups (moisture). The band at 2914 cm^{-1} was related to the C–H stretching, 1394 cm^{-1} was related to C–H bending, and 1107 cm^{-1} was due to C–O bond stretching. The band at 600 cm^{-1} corresponds to the presence of metal–oxygen (M–O), i.e., the stretching vibration of Cu_4O_3 NPs.

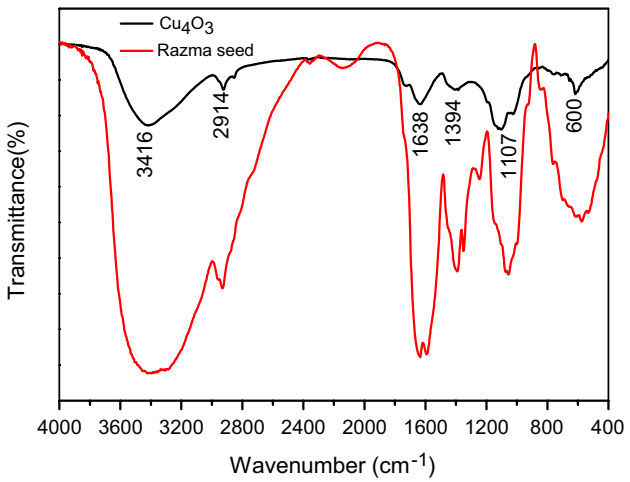

Fig. 2 FTIR spectrum of biosynthesized Cu_4O_3 NPs and Razma seed extract

3.3 Morphological studies

The scanning electron microscopy (SEM) images of as prepared Cu_4O_3 NPs are shown in Fig. 3a, b. The images reveal that Cu_4O_3 NPs are sponge-like structures with agglomeration. The elemental composition of the synthesized sample was analyzed with EDAX (Fig. 3c). The EDAX spectrum shows the presence of only copper and oxygen, indicating the purity of the sample.

Figure 4a–d shows the TEM images of the synthesized Cu_4O_3 NPs. The majority of the particles were in the range of 20–30 nm, the average size of the particles is 27 nm, and we can observe the oval-shaped particles with length of around 40 nm with the width of 20 nm. Figure 4e shows the HR-TEM image of Cu_4O_3; from this, it is clear that this material is a highly crystalline material with the obtained d-spacing value 0.42 nm which is belongs to the plane (202). Figure 4f indicates the selected area electron diffraction (SAED) pattern of Cu_4O_3 NPs. The bright spot in the selected area electron diffraction (SAED) pattern gives the crystalline nature of Cu_4O_3. The d-spacing values and hkl values calculated by the XRD and HR-TEM were well matched with those of the selected area electron diffraction (SAED) pattern.

3.4 Optical studies

Figure 5 shows the UV–visible spectrum taken at room temperature of Cu_4O_3 NPs synthesized by Razma seed extract. Spectrum revealed the characteristic absorption peaks at the wavelength 270 and 372 nm. This pattern of absorption spectrum was assigned to the intrinsic band gap absorption of Cu_4O_3 due to the electron transitions from the valence band to conduction band [31, 32]. The band gap of the Cu_4O_3 NPs was calculated from this absorption spectrum using Tauc Eq. (3) [33].

$$\alpha h\nu = D\left(h\nu - E_g\right)^n \tag{3}$$

where h is the energy of the photon, E_g is the band gap of the material and D is a constant. The band gap was found to be 4.5 and 3.3 eV for 270 and 372 nm, respectively, which is greater than that of the bulk Cu_4O_3, and it is a UV-active material. This band gap enhancement arises due to the size effect of the NPs. In addition, this sharp peak indicates that the particles are in nanosize, and the particle size distribution is narrow. A normal way to obtain the band gap from absorbance spectra is to get the first derivative of the absorbance with respect to photon

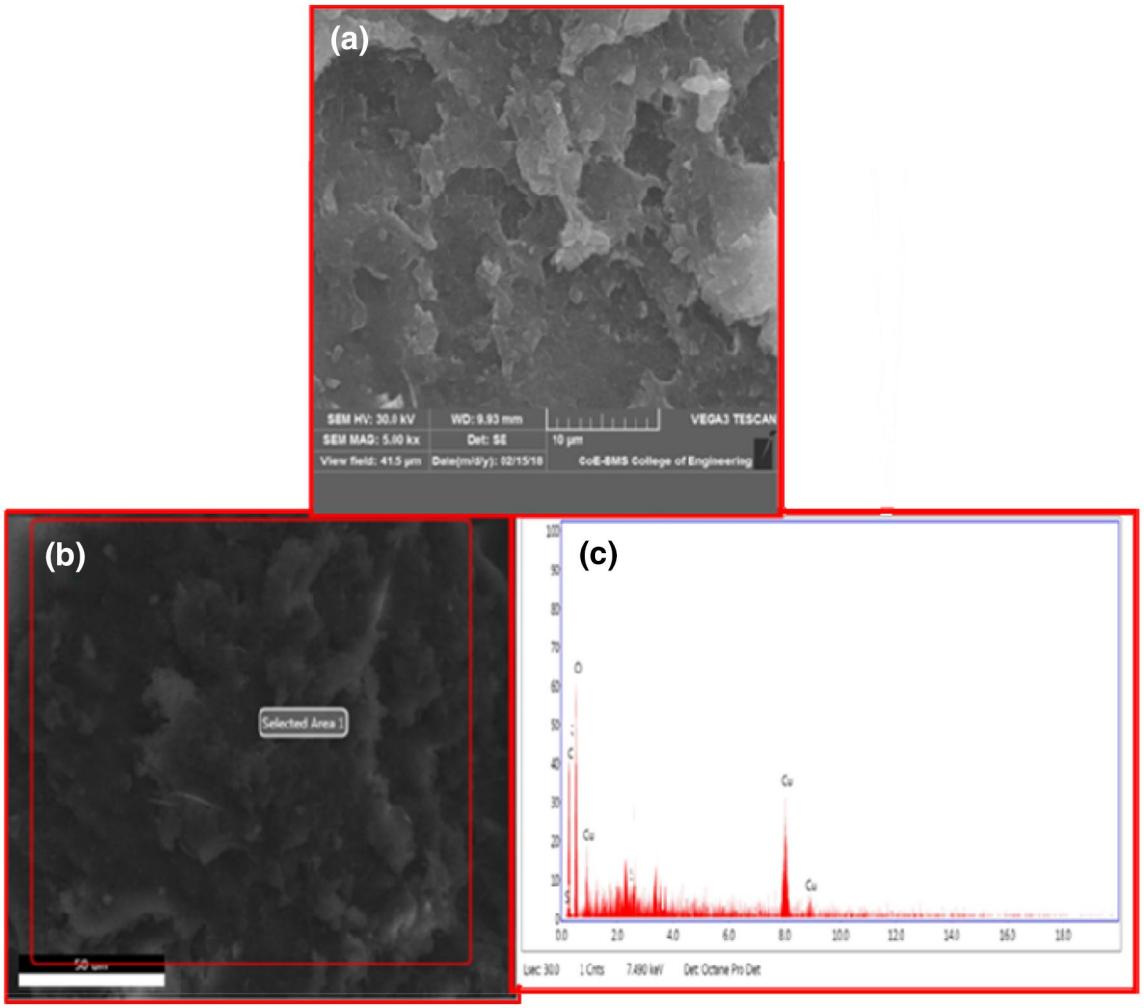

Fig. 3 **a**, **b** SEM, **c** EDAX images of Cu_4O_3 NPs

energy and find the maximum in the derivative spectrum at lower-energy sides [34, 35].

3.5 Antibacterial studies

3.5.1 Variation in susceptibility between the selected strains

The survival rate of bacteria decreased with increasing concentration of Cu_4O_3 nanoparticles. *S. aureus* (Gram-positive bacteria) and *E. coli* (Gram-negative bacteria) showed inhibition zone at the concentration 400 µg/mL and 600 µg/mL of Cu_4O_3 nanoparticles. The corresponding zone of inhibition for *E. coli* was 10 ± 0.2 mm for 400 µg/mL and 6 mm for 600 µg/mL. In case of *S. aureus*, the zone of inhibition was 5 mm for 400 µg/mL and 10 mm for 600 µg/mL. Standard ciprofloxacin antibiotic showed 20 mm zone of inhibition for both *E. coli* and *S. aureus*. Comparatively, antibiotic showed more inhibition than Cu_4O_3 nanoparticles. For inhibiting the bacteria, *E. coli* required less concentration (400 µg/mL) and *S. aureus* required more concentration (600 µg/mL) of Cu_4O_3 nanoparticles, because Gram +ve *S. aureus*, the cell wall is thick (15–80 nm) and Gram –ve *E. coli*, the cell wall is relatively thin (2–7 nm). Additionally, it also depends on size and shape of nanoparticles. *E. coli* required less concentration (400 µg/mL) of Cu_4O_3 nanoparticles for higher rate inhibition, where as *S. aureus* required higher concentration (600 µg/mL), respectively. This is due to variation in the membrane structure, size and shape of nanoparticles. Thus, morphology of Cu_4O_3 nanoparticles was spherical in shape. The penetration of nanoparticles by *E. coli* and *S. aureus* varies with different concentrations [36].

The antibacterial activity of Cu_4O_3 NPs was determined against human pathogenic bacteria comprising Gram-positive bacteria (*S. aureus*) and Gram-negative bacteria (*E. coli*), as shown in Fig. 6. The sizes of the zones of inhibition obtained with the pathogens are presented

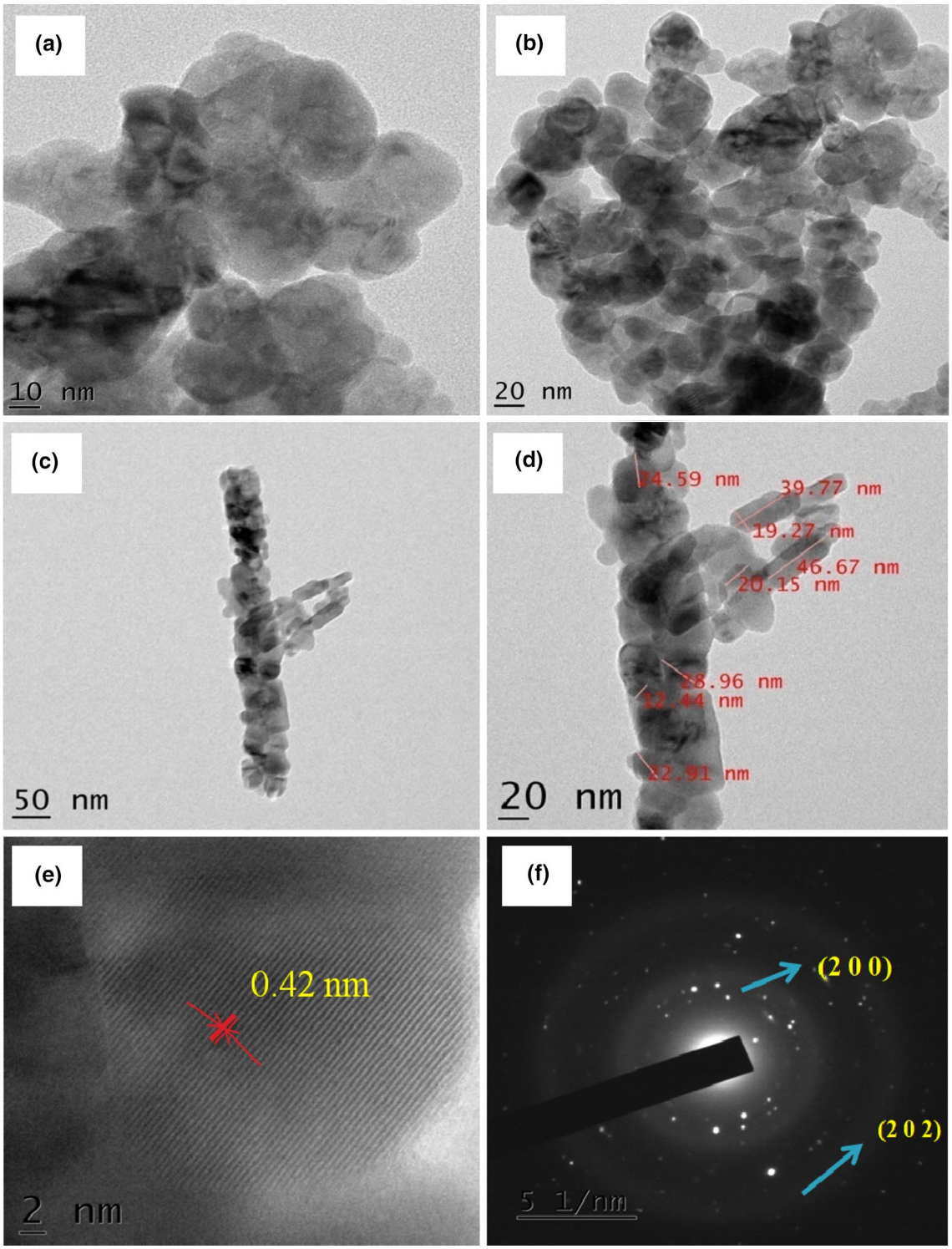

Fig. 4 TEM images (**a**–**d**), HR-TEM (**e**) and SAED pattern (**f**) of Cu_4O_3 NPs

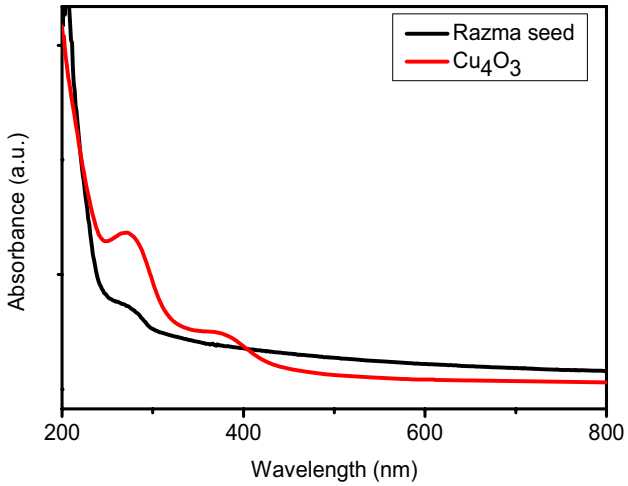

Fig. 5 UV–Vis absorbance spectrum of Cu_4O_3 NPs; NNP—nanoparticles

in Table 1. Two different pathways for antibacterial mechanism of Cu_4O_3 NPs have been reported by various researchers as discussed below, and the cell death and membrane leakage are due to the release of Cu^{2+} ions and production of reactive oxygen species. The smaller particle size gives more reactive surface area to interact with the bacteria, enhancing a better antibacterial efficiency [37, 38]. Generally, the effect of antibacterial activity depends on their morphology, specific surface area (SSA), size, charges and reactive oxygen species (ROS) [39]. When the heavy metal ions Cu^{2+} released by Cu_4O_3 NPs, surface gets into connection with the microbe cell membranes. The cell membranes with negative charge and Cu^{2+} with positive charge mutually attract, and the Cu^{2+} penetrates into the cell membrane and reacts with sulfhydryl (S–H) groups inside the cell membrane. As a result, the microbe becomes so damaged that the cells lose the ability of growth through cell division, which leads to the death of the microbe [40, 41].

3.5.2 Mechanism of antibacterial activity

From the literature survey on mechanism for antibacterial activity by different ions of copper, Cu(II) plays the major role than other Cu ions [Cu(0) and Cu(I)].

In the antibacterial activity, Cu ions involved in the killing process of bacteria by inducing the generation of reactive oxygen species (ROS), which causes cell damage [42]. The generation of ROS is probably mediated by redox cycling between the different copper species: Cu(0), Cu(I) and Cu(II). The stress caused by ROS is another factor contributing to contact killing. DNA is a major target of copper toxicity, leading to rapid DNA fragmentation and cell death. It is likely that DNA damage ensures only as a secondary event following cell death. Metal-bacterial contact damages the cell envelop which in turn makes the cells susceptible to further damage by copper ions [42].

In addition, Cu ions enter into the agar plate and kill the bacteria or inhibit the bacterial growth. The insertion of Cu ions into the cells eventually changes the ion concentration and causes leakage of DNA and RNA, and inactivation of enzyme thus kills the bacteria.

The strong antibacterial activity of Cu ions is due to inhibition of dehydrogenase activity of bacterial population by nano-Cu and $CuCl_2$, elevated copper levels inside a cell cause oxidative stress and the generation of hydrogen peroxide participates in Fenton-type reaction, causing oxidative damage to cells.

Excess copper causes a decline in the membrane integrity of microbes, leading to leakage of specific essential cell nutrients, such as potassium and glutamate, which leads to desiccation and subsequent cell death [43]. The redox properties of copper can also cause cellular damage due to the generation of reactive hydroxyl radicals (Fenton-type reaction).

$$Cu^{+} + H_2O_2 \rightarrow Cu^{2+} + OH^{\cdot} + OH^{-}$$

The generated reactive hydroxyl radicals can participate in the oxidation of proteins and lipids. Those copper ions

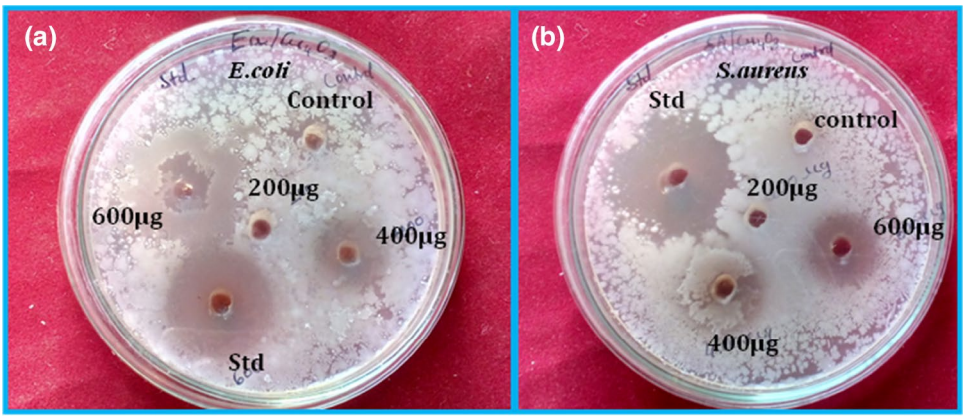

Fig. 6 Antibacterial activity: **a** *Escherichia coli*, b *Staphylococcus aureus*

can lead to the depletion of sulfhydryls, such as cysteines, and finally leads to damage to the cell [43].

The antibacterial activities of the Cu_4O_3 were evaluated by means of Gram-positive (+ve) and Gram-negative (−ve) bacteria [44]. Cu^{2+} could be the active species for copper oxide antibacterial materials, responsible for the antibacterial activity. Cu^{2+} ions released from copper oxides may produce hazardous effects by generating the reactive oxygen species (ROS), for instance $O_2^{2-\cdot}$, $^{\cdot}OH$ and $HO_2^{-\cdot}$ which damage the cytomembrane and then disrupt amino acid synthesis and DNA. The ROS could be generated from the surface defect sites in the Cu_4O_3 NPs or induced by the high concentrations of free Cu^{2+} ions released from the Cu_4O_3 NPs. With increasing quantity of the Cu_4O_3 from 200 µg to 600 µg, the concentrations of Cu^{2+} ions increase near linearly. The satisfying antibacterial rates are achieved. These results indicate there is a critical value for the Cu^{2+} concentration and the growth of bacteria can be effectively inhibited as long as the Cu^{2+} concentration reaches the critical value. The critical concentrations of the Cu^{2+} are different for different bacteria due to the difference in antibacterial activities.

Cu^{2+} ions released from the Cu_4O_3 were responsible for the antibacterial activity. Copper facilitates deleterious activity in superoxide radicals. Repeated redox reactions on site-specific macromolecules generate HO• radicals, thereby causing "multiple hit damage" at target sites; it results in death of bacteria [44].

3.6 Anticancer studies

3.6.1 Working principle

Based on the literature survey, the mechanism has been explained below.

Passive targeting by nanoparticles

The enhanced permeability and retention (EPR) effect is usually applied to NPs delivered to cancer tissues. In EPR effect, the molecules of certain sizes typically nanoparticles and macromolecular drugs tend to accumulate in tumor tissue much more than the normal tissues because tumor cells grow quickly; they stimulate the production of blood vessels, and vascular endothelial growth factors are involved in cancer angiogenesis. Tumor cell aggregates as small as 150–200 µm. Fast-growing cancer cells demand the recruitment of new vessel neovascularization (the formation of new blood vessels) or rerouting of existing vessels near the tumor mass to supply them with oxygen and nutrients. These newly formed tumor vessels are usually abnormal in form and shapes; they poorly align defective endothelial cells with wide fenestrations, and tumor tissues usually lack effective lymphatic drainage. The resulting imbalance of angiogenic regulators such as growth factors and matrix metalloproteinases makes tumor vessels highly disorganized and dilated with numerous pores showing enlarged gap junctions between endothelial cells.

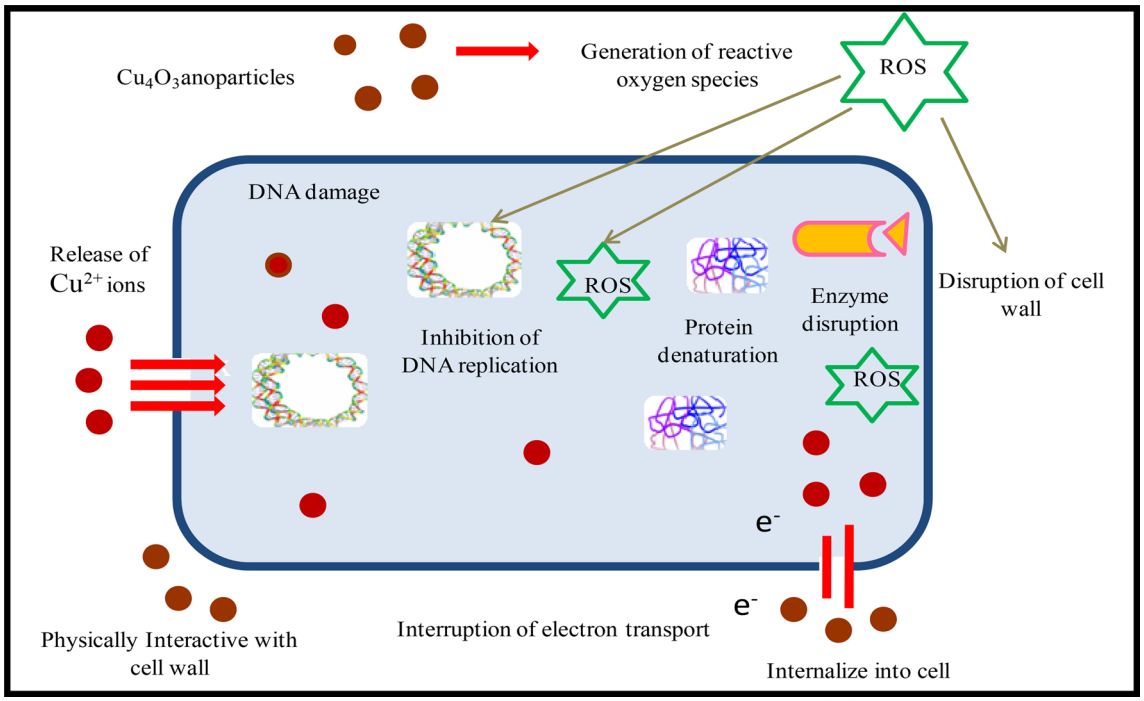

Fig. 7 Antibacterial mechanism of biosynthesized Cu_4O_3 NPs

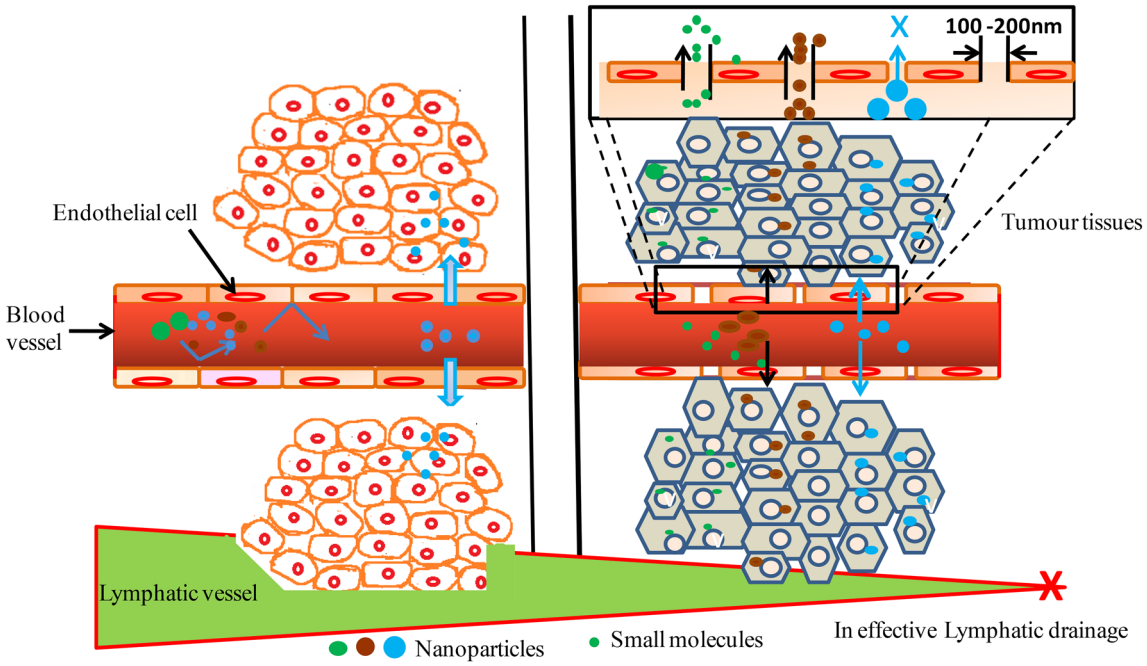

Fig. 8 Differences between normal and tumor tissues that explain the passive targeting of nanoparticles by the enhanced permeability and retention effect

These features are called the enhanced permeability and retention effect, and macromolecules and nanoparticles, with a molecular weight above 50 kDa, can selectively accumulate in the tumor interstitium. Normally, tissues endothelial cells form a single layer, there are no numerous pores and gap junctions between endothelial cells and the NPs do not easily penetrate into normal tissues. The nanoparticles affect only tumor tissue [45] (Fig. 7).

3.6.2 Measurement of cytotoxicity by MTT assay

The present work agrees with the desired application for cancer treatment. Anticancer activity in terms of the cell viability against PC-3 cell line and normal cell line is presented in Fig. 8. Viability of cancer and normal cells against Cu_4O_3 NPs was examined by MTT assay. Cytotoxic activity of Cu_4O_3 NPs was analyzed against NIH 3T3 normal cell line and PC-3 cancer cell line. The inhibitory activity of against normal and cancer cell lines was detected using different concentrations of Cu_4O_3 NPs (20, 40, 60, 80, 100 µg/mL), and viability (%) of the cells was determined

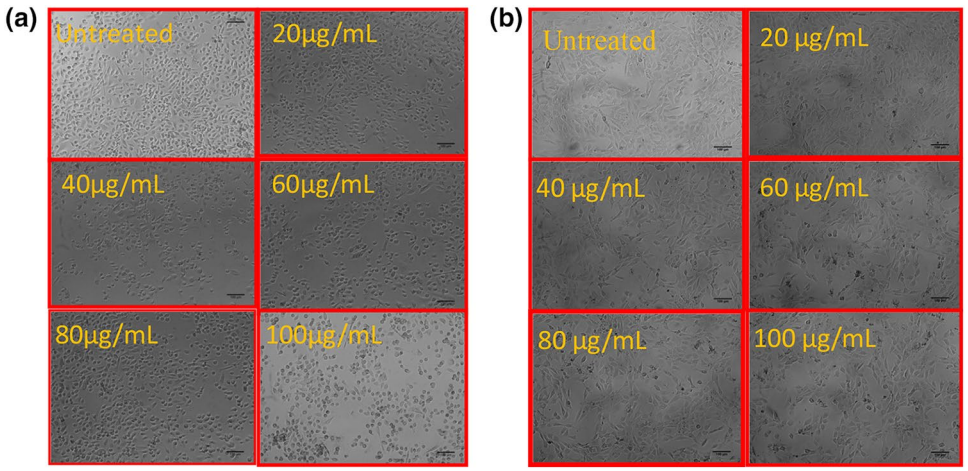

Fig. 9 **a** Cytotoxicity of Cu_4O_3 NPs against human prostate cancer cell line (PC-3), **b** cytotoxicity of Cu_4O_3 NPs against NIH/3T3 cell line (normal cell line)

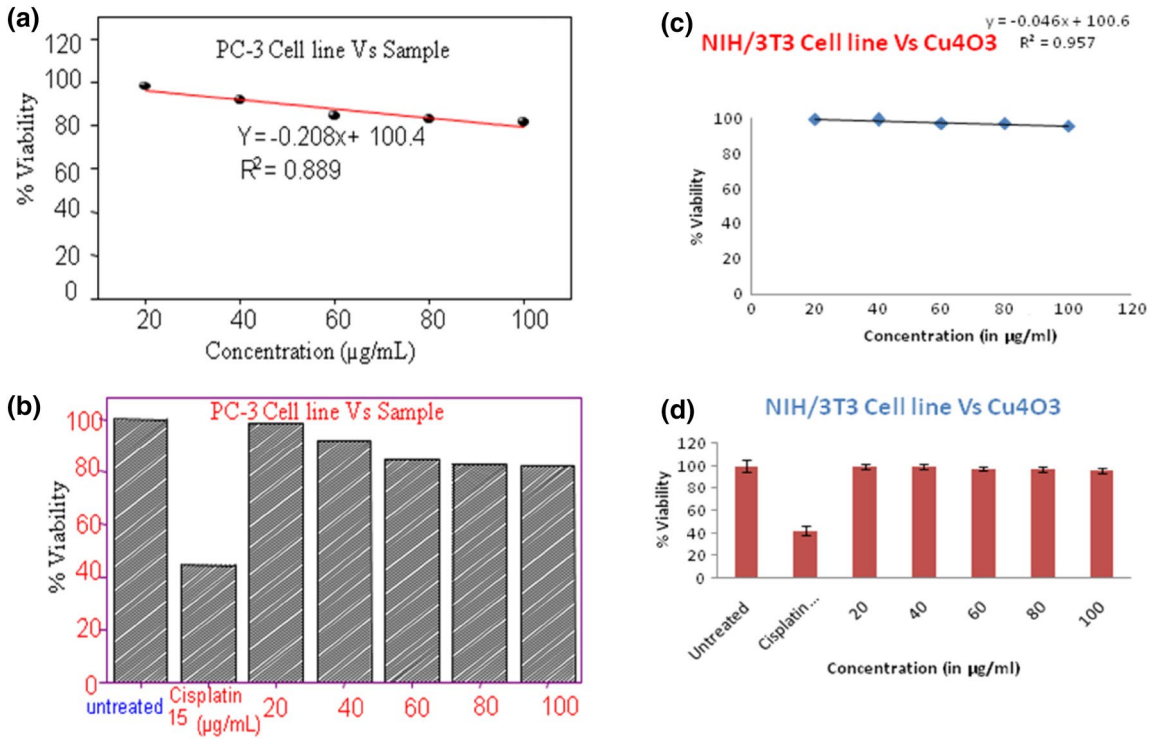

Fig. 10 **a**, **b** Percentage of cell inhibition in human prostate cancer cell line PC-3 with different concentrations of Cu_4O_3. **c**–**d** Percentage of cell inhibition in NIH/3T3 Cell line (normal cell line) with different concentrations of Cu_4O_3

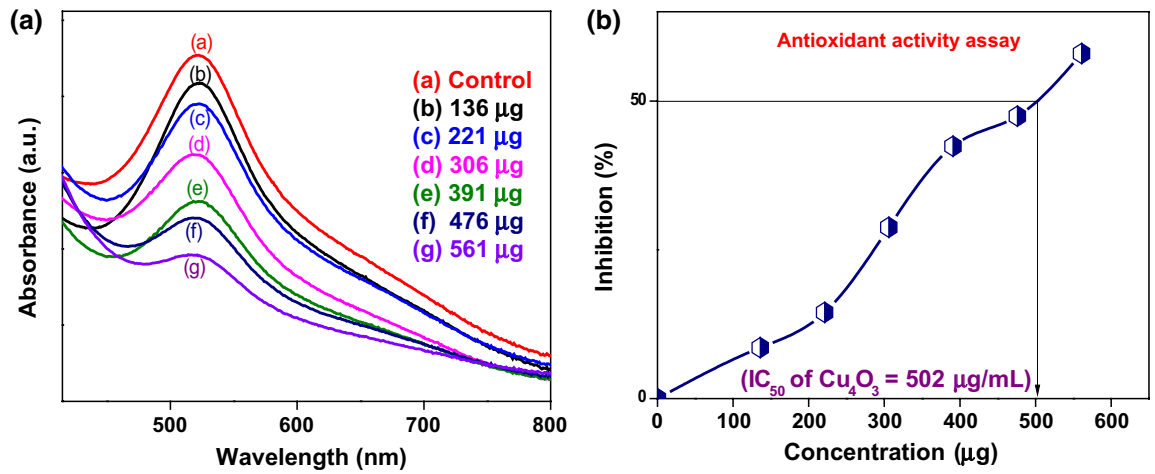

Fig. 11 **a** UV–Vis spectrum of DPPH solution with different concentrations of Cu_4O_3 and **b** graph of IC_{50} value of Cu_4O_3 NP concentration (µg/mL)

by colorimetric method. MTT results showed that Cu_4O_3 NPs significantly decreased the viability of cancer cell line in a dose-dependent manner (20-100 µg/mL) and the inhibitory concentration (IC_{50}) was found to be 241.83 µg/mL. However, Cu_4O_3 NPs did not induce significant reduction in the viability of normal cells with concentration of 20-100 µg/mL. The obtained results clearly revealed that Cu_4O_3 NPs greatly kill the cancer cells and have less affect on normal cell lines. Cu_4O_3 nanoparticles have been used in biomedical applications including chemotherapy and drug delivery. Hence, Cu_4O_3 NPs provide a promising tool in cancer therapy [46] (Figs. 9, 10, 11).

3.7 Antioxidant activity studies

The DPPH, a stable free radical with a characteristic absorption at 520 nm, was used to study the radical scavenging activity of Cu_4O_3 NPs. The decrease in absorption is considered as a measure of the extent of radical scavenging. The percentage of inhibition or scavenging of free radicals was determined. The Cu_4O_3 NPs were inhibiting the DPPH free radical scavenging activity with IC_{50} value of 502 µg/mL as shown in Fig. 9b.

4 Conclusion

In the present work, biosynthesis method was employed to obtain paramelaconite tetragonal copper oxide (Cu_4O_3) NPs from the assistance of Razma seed extract as a green reducing/stabilizing agent. XRD, FTIR, SEM, TEM and UV–Vis techniques were utilized to characterize the as-synthesized nanoparticles. SEM and TEM images reveal that nanoparticles possess sponge-like structures with more or less spherical shape. The average particle size was found to be 27 nm. Cu_4O_3 NPs exhibited significant antibacterial activity against the food-borne pathogens (S. *aureus and E. coli*). Furthermore, the cytotoxic activity of the Cu_4O_3 NPs was high against the prostate cancer cell line (PC-3) with IC_{50} value of 241.83 µg/mL. Cu_4O_3 nanoparticles exhibited a significant antioxidant activity. Overall, the biosynthesized Cu_4O_3 nanoparticles will be useful in biomedical applications (food packaging and pharmaceutical industries).

Compliance with ethical standards

Conflict of interest The authors declare that they have no conflict of interest.

References

1. Firdhouse MJ, Lalitha P (2013) Biosynthesis of silver nanoparticles using the extract of *Alternanthera sessils*—antiproliferative effect against prostate cancer cells. Cancer Nanotechnol 4:137–143
2. Mbeunkui F, Johann DJ Jr (2009) Cancer and the tumor micro environment: a review of an essential relationship. Cancer Chemother Pharmol 63:571–582
3. Karthik K, Dhanuskodi S, Gobinath C, Prabukumar S, Sivaramakrishnan S (2018) Nanostructured CdO–NiO composite for multifunctional applications. J Phys Chem Solids 112:106–118
4. Ramasubburayan R, Sumathi S, Bercy DM, Immanuel G, Palavesam A (2015) Antimicrobial, antioxidant and anticancer activities of mangrove associated bacterium *Bacillus subtilis* subsp, Subtilis RG. Biocatal Agric Biotechnol 4:158–165
5. Suresh D, Udayabhanu, Nethravathi PC, Lingaraju K, Raja Naika H, Sharma SC, Nagabhushana H (2015) EGCG assisted green synthesis of ZnO nanopowders: photodegradative, antimicrobial and antioxidant activities. Spectrochim Acta Part A Mol Biomol Spectrosc 136:1467–1474
6. Suresh D, Nethravathi PC, Udayabhanu, Kumar MAP, Naik HR, Nagabhushana H, Sharma SC (2015) Chironji mediated facile green synthesis of ZnO nanoparticles and their photoluminescence, photodegradative, antimicrobial and antioxidant activities. Mater Sci Semicond Process 40:759–765
7. Suresh D, Nethravathi PC, Udayabhanu, Raja Naika H, Nagabhushana H, Sharma SC (2015) Green synthesis of multifunctional zinc oxide (ZnO) nanoparticles using *Cassia fistula* plant extract and their photodegradative, antioxidant and antibacterial activities. Mater Sci Semicond Process 31:446–454
8. Pinilla CMB, Brandelli A (2016) Antimicrobial activity of nano liposomes co-encapsulating nisin and garlic extract against Gram-positive and Gram-negative bacteria in milk. Innov Food Sci Emerg Technol 36:287–293
9. Wang C, Cheng X, Zhou X, Sun P, Hu X, Shimanoe K, Lu G, Yamazoe N (2014) Hierarchical α-Fe_2O_3/NiO nanocomposites with a hollow structure for a gas sensor. ACS Appl Mater Interfaces 6:12031–12037
10. Karthik K, Dhanuskodi S, Gobinath C, Prabukumar S, Sivaramakrishnan S (2017) Dielectric and antibacterial studies of microwave assisted calcium hydroxide nanoparticles. J Mater Sci: Mater Electron. https://doi.org/10.1007/s10854-017-7563-5
11. Akbar A, Sadiq MB, Ali I, Muhammad N, Rehman Z, Khan MN, Muhammad J, Khan SA, Rehman FU, Anal AK (2019) Synthesis and antimicrobial activity of Zinc oxide nanoparticles against foodborne pathogens *Salmonella typhimurium* and *Staphylococcus aureus*. Biocatal Agric Biotecnol 17:36–42
12. Revathi S, Govindarajan RK, Rameshkumar N, Hakkim FL, Mohammed A-B, Krishnan M, Kayalvizhi N (2017) Anticancer, anti-microbial and anti-oxidant properties of *Acacia nilotica* and their chemical profiling. Biocatal Agric Biotechnol 11:322–329
13. Revanna RH, Panchangam RK, Bhanu U, Doddavenkatanna S (2016) Synthesis, characterization and in vitro antioxidant activity of new chiral N-boc organotellurium compounds, $(CH_3)_3OC(O)NHCH(R)C(O)NHCH_2–CH_2$ $Te–C_6H_4–4–OCH_3$, containing carbamate and peptide groups. J Braz Chem Soc 27:1157–1164
14. Nabila MI, Kannabiran K (2018) Biosynthesis, characterization and antibacterial activity of copper oxide nanoparticles (CuO NPs) from actinomycetes Biocatal. Agric Biotechnol 15:56–62
15. Murali DS, Subrahmanyam A (2016) Synthesis of low resistive p type Cu_4O_3 thin films by DC reactive magnetron sputtering and conversion of Cu_4O_3 into CuO by laser irradiation. J Phys D Appl Phys 49:375102
16. Wang Y, Ghanbaja J, Soldera F, Migot S, Boulet P, Horwat D, Mücklich F, Piers JF (2015) Tuning the structure and preferred orientation in reactively sputtered copper oxide thin films. Appl Surf Sci 335:85–91
17. Pierson JF, Duverger E, Banakh O (2007) Experimental and theoretical contributions to the determination of optical properties of synthetic paramelaconite. J Solid State Chem 180:968–973
18. Debbichi L, Marco de Lucas MC, Pierson JF, Kriiger P (2012) Vibrational properties of CuO and Cu_4O_3 from first-principles calculations, and Raman and infrared spectroscopy. J Phys Chem C 116:10232–10237
19. Murali DS, Subrahmanyam A (2016) Synthesis of low resistive p type (Cu_4O_3), thin films by DC reactive magnetron sputtering and conversion of (Cu_4O_3) into CuO by laser irradiation. J Phys D Appl Phys 49:375102

20. Jiang Z, Tiang S, Lai S, McAuliffe RD, Rogers SP, Shim M, Shoemaker DP (2016) Capturing phase evolution during solvothermal synthesis of metastable (Cu_4O_3). Chem Mater 28:3080–3089
21. Whangbo MH, Koo HJ (2002) Spin dimer analysis of the spin exchange interactions in paramelaconite Cu_4O_3 and its analogue $Ag_2Cu_2O_3$ and the spin ordering of the Cu_2O_3 spin lattice leading to their magnetic phase transitions. Inorg Chem 41:3570–3577
22. Zhao L, Chen H, Wang Y, Che H, Gunawan P, Zhong Z, Li H, Su F (2012) Facile solvothermal synthesis of phase—pure Cu_4O_3 microspheres and their lithium storage properties. Chem Mater 24:1136–1142
23. Almasi H, Jafar Zadeh P, Mehryar L (2018) Fabrication of novel nonohybrids by impregnation of Cuo nanoparticles into bacterial cellulose and chitosan nanofibers: characterization, antimicrobial and release properties. Corbohydr Polym 186:273–281
24. Lingaraju K, Raja Naika H, Nagabhushana H, Nagaraju G (2018) *Euphorbia heterophylla* (L.) mediated fabrication of ZnO NPs: characterization and evaluation of antibacterial and anticancer properties. Biocatal Agric Biotechnol 18:100894
25. Raja Naika H, Lingaraju K, Manjunath K, Kumar Danith, Nagaraju G, Suresh D, Nagabhushana H (2015) Green synthesis of CuO nanoparticles using *Gloriosa superb* L. Extract and their antibacterial activity. J Taibah Univ Sci 9:7–12
26. Narendran R, Kathiresan K (2016) Antimicrobial activity of crude extracts from Mangrove-derived Trichoderma species against human and fish pathogens. Biocatal Agric Biotechnol 6:189–194
27. Halim NRA, Azlan A, Yusof HM, Sarbon NM (2018) Antioxidant and anticancer activities of enzymatic eel (*Monopterus* sp.) protein hydrolysate as influenced by different molecular weight. Biocatal Agric Biotechnol 16:10–16
28. Williams WB (1995) Protein extraction from plant tissue in methods in molecular biology, protein purification protocols. Food Sci Techol 28:23–30
29. Suresh D, Udayabhanu, Nagabhushana H, Sharma SC (2015) Clove extract mediated facile green reduction of grapheme oxide, its dye elimination and antioxidant properties. Mater Lett 142:4–6
30. Suresha D, Nethravathia PC, Udayabhanua U, Nagabhushana H, Sharma SC (2015) Spinach assisted green reduction of grapheme oxide and its antioxidant and dye absorption properties. Ceram Int 141:4810–4813
31. Zak AK, Majid WHA, Mahmoudian MR, Darroudi M, Yousefi R (2013) Starch-stabilized synthesis of ZnO nanopowders at low temperature and optical properties study. Adv Powder Technol 24:618–624
32. Khorsand Zak A, Yousefi R, Majid WHA, Muhamad MR (2012) Antioxidant and anticancer activities of enzymatic eel (*Monopterus* sp.) protein hydrolysate as influenced by different molecular weight. Ceram Int 38:059–2064
33. Nudelman S (1969) Optical properties of solids. Plenum Pub Corp
34. Khorsand AZ, Razali R, Majid WHA, Darroundi M (2011) Synthesis and characterization of a narrow size distribution of zinc oxide nanoparticles. Int J Nanomed 6:1399–1403
35. Udayabhanu, Nethravathi PC, Kumar MAP, Suresh D, Lingaraju K, Raja Naika H, Nagabhushana, Sharma (2015) *Tinospora cordifolia* mediated facile green synthesis of cupric oxide nanoparticles and their photocatalytic, antioxidant and antibacterial properties. Mater Sci Semicond Process 33:81–88
36. Azam A, Ahmed AS, Oves M, Khan MS, Habib SS, Memic A (2012) Antimicrobial activity of metal oxide nanoparticles against Gram-positive and Gram-negative bacteria: a comparative study. Int J Nanomed 7:6003–6009
37. Revathi V, Karthik K (2018) Microwave assisted CdO–ZnO–MgO nanoparticles and its photocatalytic and antibacterial studies. J Mater Sci: Mater Electron 29:18519–18530
38. Jagathesan G, Rajiv P (2018) Biosynthesis and characterization of iron oxide nanoparticles using Eichhornia crassipes leaf extract and assessing their antibacterial activity. Biocatal Agric Biotechnol 13:90–94
39. Karthik K, Dhanuskodi S, Gobinath CS, Prabukumar S, Sivaramakrishnan S (2018) Multifunctional properties of CdO nanostructures synthesised through microwave assisted hydrothermal method. Mater Res Innov. https://doi.org/10.1080/14328917
40. Karthik K, Dhanuskodi S, Gobinath C, Sivaramakrishnan S (2015) Microwave-assistted synthesis of CdO–ZnO nanocomposite and its antibacterial activity against human pathogens. J Mol Spectrosc 139:7–12
41. Naik MM, Naika HSB, Nagaraju G, Vinuth M, Vinu K, Rashmi SK (2018) Effect of aluminium doping on structural, optical, photocatalytic and antibacterial activity on nickel ferrite nanoparticles by sol-gel auto-combustion method. J Mater Sci: Mater Electron 29(23):20395–20414
42. Ciacotich N, Kragh KN, Lichtenberg M, Tesdorpf JE, Bjarnsholt T, Gram L (2019) In situ monitaring of the antibacterial activity of a copper–silver alloy using confocal laser scanning microscopy and pH microsensors. Antibact Coat Glob Chall. https://doi.org/10.1002/gch2.201900044
43. Grass G, Rensing C, Solioz M (2011) Metallic copper as an antimicrobial surface. Appl Environ Microbiol 77:1541–1547
44. Wang W, Zhu L, Lv P, Liu G, Yu, Li J (2018) Novel Candy-like Cu_4O_3 microstructure: facile wet chemical synthesis, formation mechanism, and good long-term antibacterial activities. ACS Appl Mater Interfaces. https://doi.org/10.1021/acsami.8b14470
45. Dand NM, Patel PB, Ayre AP, Kadam VJ (2013) Polymeric micelles as a drug for tumor targeting. Chron Young Sci 4:94–101
46. Karthik K, Dhanuskodi S, Gobinath C, Prabukumar S, Sivaramkrishnan S (2019) Fabrication of MgO nanostructures and its efficient photocatalytic, antibacterial and anticancer performance. J Photochem Photobiol B Biol 190:8–20